

Assignment

Homelab HL4

Alberto Doimo 10865196

Riccardo Iacecarino 10868500

Musical Acoustics



POLITECNICO
MILANO 1863

January 22, 2024

Introduction

In this report we will discuss the implementation of a 4-steps model of a trumpet in COMSOL Multiphysics in order to simulate its acoustic response. In particular we will start with the study of a tube, to which it will be then attached a bell; the third part is instead focused on the mouthpiece, that is finally combined with the other components to complete the instrument. Since most of the procedures to be performed in order to correctly model the elements do not depend on the specific case, we will now provide an overview of the general process. Thanks to the instrument's axial symmetry, we can exploit the *2D axisymmetric* option, which drastically reduces computational costs and therefore simulation time. Furthermore we will base our simulations on the *Pressure Acoustics, Frequency Domain* physics, which allows us to study acoustic waves and in particular their propagation in fluids. It also exploits frequency domain studies in order to collect different responses of the system at once, making the identification of eigenfrequencies a trivial operation. Indeed, we will analyze the input impedance of the 4 configurations as the ratio between pressure and acoustic velocity, both quantities obtained from the COMSOL's studies. The last part of each exercise is instead focused on the directivity properties of the system: polar plots at significant frequencies will be computed and commented to investigate the behaviour of the instrument as a function of the observation direction.

1) Impedance of a tube

The first subject of our study is a simple tube, which will later be the body of the trumpet. Thanks to the axisymmetric functionality, we can draw the model in a plane, which will be then rotated around the z-axis to obtain the 3D system.

Name	Expression	Value	Description
rT	0.6[cm]	0.006 m	Tube radius
rS	2[m]	2 m	Air sphere radius
N	255	255	Number of frequencies
Lt	1.37[m]	1.37 m	Tube length
Lspace	20[mm]	0.02 m	Length empty space
lambdaMax	c0/fMax	0.08575 m	Wave length max frequency
fMin	50[Hz]	50 Hz	Min Frequency
fMax	4000[Hz]	4000 Hz	Max Frequency
c0	343[m/s]	343 m/s	wave speed

Figure 1: Simulation parameters for the tube

Following the parameters indicated in Fig.1 we start creating the geometry of Fig.2 with a rectangular object ($rT \times Lt$) whose upper surface is located at $z = 0$. Immediately below the tube, another rectangle ($rT \times Lspace$) is sketched in order to model a discontinuity that will be later useful to correctly apply the input pressure. Specifically it will be removed from the geometry, hence avoiding the propagation of a wave downwards, outside of the tube.

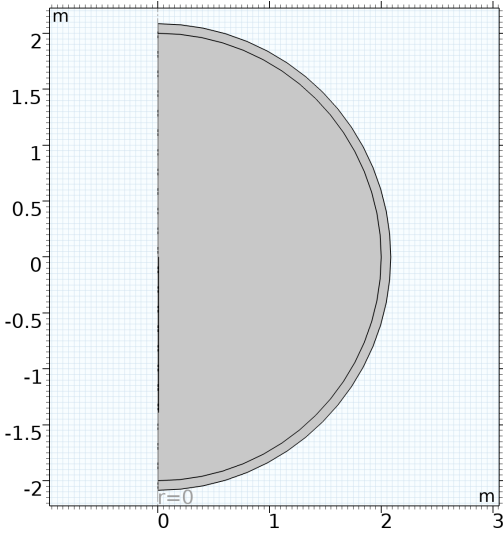


Figure 2: 2D geometry of the tube

Two circumferences (with their center in the origin) are then placed around the geometry: the inner one, of radius rS , will model the air volume in which the instrument lies; the outer is instead increased of $\text{LambdaMax} = 0.28583 \text{ [m]}$ w.r.t. the other and it will be fundamental for the simulation of free field conditions. Speaking of which, we can introduce the *Perfectly Matched Layer* (PML), an artificial domain condition imposed on the external portion of the volume, namely the one that is in between the circumferences. This portion is responsible for emulating an open and infinite domain, and we can achieve the desired behaviour by validating two conditions:

- the PML thickness is set to be equal to LambdaMax , in particular we found that one wavelength is already enough if correctly meshed, but in other applications also multiples of the wavelength of the highest frequency are considered.
- the distance between the PML and the source (located at the origin) must be larger than $\lambda/8$. This condition is satisfied by the dimension of the sphere even at low frequencies.

The next step involves meshing the 2D model, imposing the requested 5 points per wavelength condition. For this purpose, the first option added in the dedicated COMSOL section is the *Size* of the mesh, which we modify as reported in Fig.3, with the maximum element dimension equal to one fifth of the smallest wavelength that we will deal with.

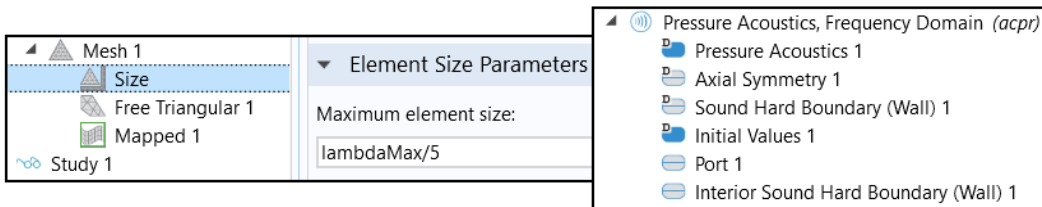


Figure 3: COMSOL options used

Now we can choose the proper mesh for our domains: in particular the *Free Triangular* has been adopted for the instrument and the air volume, whereas the *Mapped* one has been added to the PML, as suggested by the developers of the software. The validity of the latter choice can be checked by looking at the number of elements generated in the PML region (Fig.4a): the optimal trade-off between computational costs and reliability of the results can be found from 4 to 6.

To the whole subject of study the material *air* has been assigned: its properties are fundamental for a correct simulation. Notice that we will use this material for each point of the assignment, but we will not mention it again to avoid repetition. The final section that we encounter before launching the simulation is related to the physics.

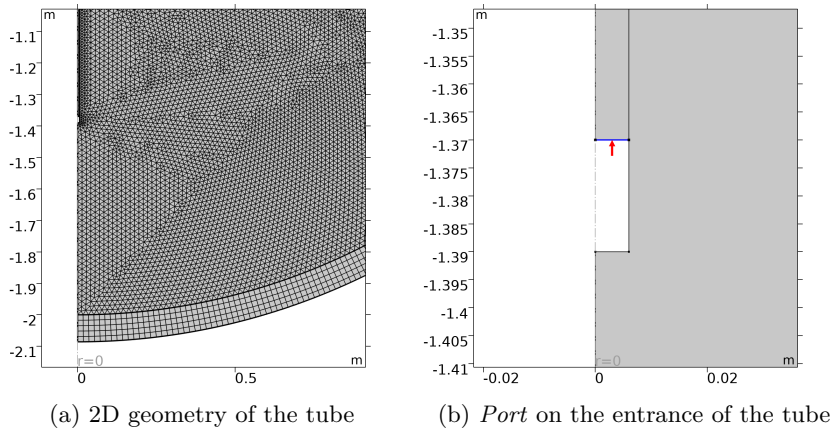


Figure 4: Model details

As already anticipated, we will rely on the *Pressure acoustics, Frequency Domain* option, in which we will characterize different boundaries and domains of the model, as shown in Fig.3. In particular with the option *Port* we can model the input pressure, which will be assigned to the "entrance" of the tube (Fig.4b) and will be set as circular with an amplitude of 1.1 [Pa]. The other important option added in the physics regards the approximation of the tube's boundaries as perfectly rigid, and can be set with the *Interior Sound Hard Boundaries* command. Finally we can focus our attention on the study: the simulation will be a *Frequency Domain* performed in the range $[f_{Min}, f_{Max}]$, with N steps linearly spaced. Two global variables (*Pressure* and *Velocity*) are added to retrieve the quantity of interest. Moreover, in order to correctly compute the impedance, a spatial *integration* is defined on the input surface. The input impedance of the tube is then computed as:

$$|Z_{in_{tube}}| = 10 \cdot \log_{10} \frac{\left| \int Pressure_{in_{tube}} \right|}{\left| \int Velocity_{in_{tube}} \right|} \quad (1)$$

and then plotted in Fig.5. The behaviour of the impedance mostly matches our expectations: it resembles the trend of the input impedance of an open-open pipe. In particular, we can appreciate from the zoom on the lowest frequencies that the first maximum is at 65.49 Hz, whereas the first minimum lies around 127.45 Hz.

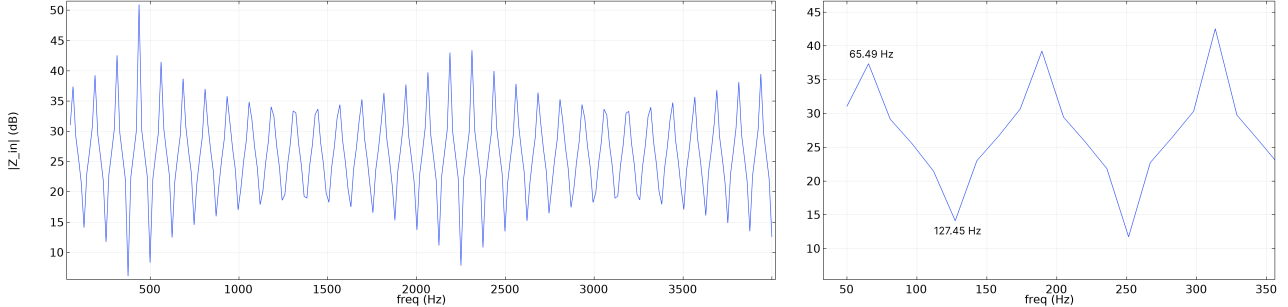


Figure 5: Input impedance of the tube and zoom on its first resonances

These values are coherent with theory, from which we can report the expressions for maxima and minima of this configuration:

$$f_{\max} = \frac{(2n - 1)c}{4Lt} \quad f_{\min} = \frac{nc}{2Lt} \quad (2)$$

In fact, for $n = 1$, we would get $f_{\max} = 62.6$ [Hz] and $f_{\min} = 125.2$ [Hz]. The deviation from the theoretical results, can be mainly associated with the relatively small amount of samples used, which causes the resonances to be detected at slightly different frequencies. Another effect caused by the limited number of samples N is the presence of an "artificial envelope" visible in particular around 1300 Hz and 3100 Hz that shapes the actual trend. In that range each resonance is composed by two samples, therefore the actual peaks are not displayed; they could be found with an increased resolution.

Moreover, from the results of the study we can also visualize how the tube radiates in the environment at different frequencies. In Fig.6 we can observe the main difference between high and low frequency: the amplitude of the pressure is greater at low frequency w.r.t. low frequency and of course the number of nodal lines is increased. From these images we can also appreciate the correct functioning of the PML, which perfectly absorbs the incident waves.

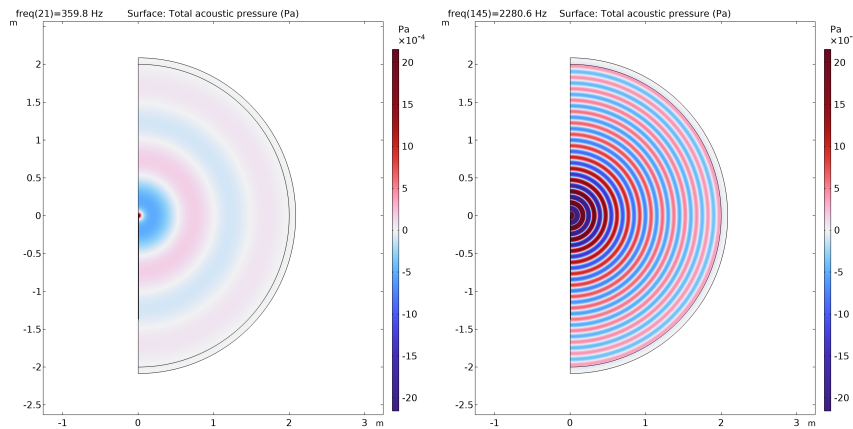


Figure 6: Total acoustic pressure simulated in the air volume

The last analysis performed on the tube regards the directivity pattern: this function

describes how the intensity of sound radiated from a source varies with direction. Even though some considerations could be drawn also from the plots of Fig.6, we will discuss in depth of the topic, and for this reason we will rely on polar plots. In order to get them, we first defined in the *Datasets* a new *Parametric Curve 3D*, which consists in a circumference that lies in the y-z plane and has its center in the origin. We can now exploit a *Polar Plot* to study the directivity of the tube at different frequencies. In particular we decided to plot the normalized SPL through the use of a *Maximum* function applied to the boundary of the sphere of radius rS , to improve readability.

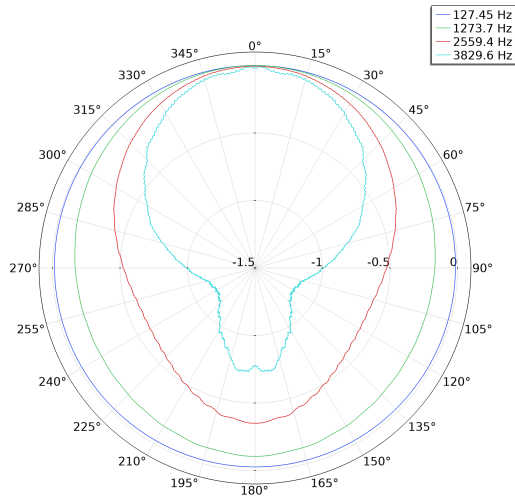


Figure 7: Polar plot of the directivity pattern of the tube (first resonance and its multiples of 10 are plotted)

From Fig.7 we can appreciate how the tube behaves as an isotropic source at low frequencies, becoming more directive when moving towards the higher end of the studied spectrum. As a matter of fact the behaviour is almost always omnidirectional if compared to the configurations analyzed later, since a decrease of just 1 dB does not make the object a very directive source.

2) Tube with bell

For the second exercise we will implement a change in the geometry with the addition of a bell on the upper side of the tube. Moreover, we will shift down the whole structure so that the end of the bell coincides with the origin of the axis, consistently with the previous study. Regarding the geometry of the new component, we can define a *Parametric Curve* of length Lh that will shape the bell following the equation:

$$r = \sqrt{\frac{St}{\pi}} e^{mz} \quad (3)$$

whose parameters can be found in Fig.8.

Name	Expression	Value	Description
Lh	0.2[m]	0.2 m	Bell length
m	28	28	Bell exponent
St	rT^2*pi	1.131E-4 m ²	Surface tube

Figure 8: Simulation parameters for the bell

The remaining parts of the *Geometry* are left untouched since all the considerations on their dimensions still hold for this configuration. The result can be appreciated in Fig.9a.

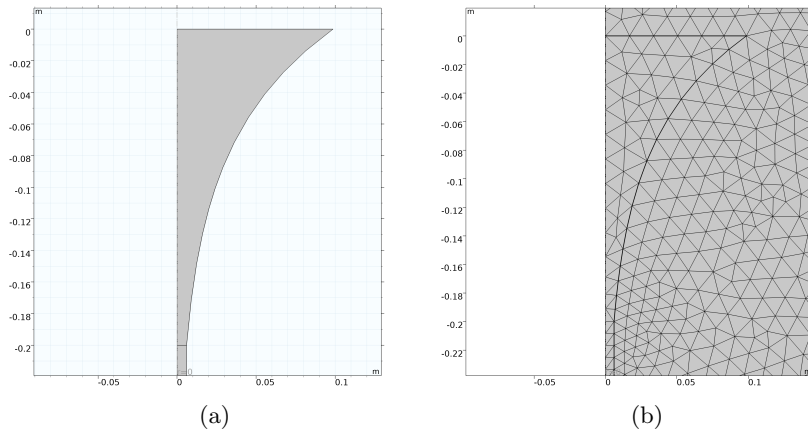


Figure 9: Bell geometry (a) and mesh (b)

Once the geometry is completed, we can move on meshing the model as we already discussed in the previous section. Specifically, the bell is now part of the instrument and so will be treated with a *Free Triangular* mesh together with the tube. Furthermore we want to highlight that there's no need to change any other parameter or meshing setting w.r.t. point 1) since the frequency range of interest does not change. In Fig.9b we can see the meshed bell.

For what regards the physics we will exploit again a *Port* on the entrance of the tube (Fig.4b) and the whole external boundary of the instrument will undergo the *Interior Sound Hard Boundaries* option.

The *Frequency Domain* study will be the very same for each configuration, and this also applies for the two *Nonlinear Couplings* (*integration* and *maximum*). At this point we can store the *Pressure* and *Velocity* variables necessary to compute the Impedance of Fig.10.

The resonant frequencies seem to be the very same of the tube, even though we cannot be certain about it due to the low resolution of the plot ($N = 255$). What changes the most with the introduction of the bell is the attenuation of higher frequencies peaks, which settle around 26 dB. We expect from theory that this behaviour also reflects in an improvement in terms of radiation, so we can immediately check the directivity pattern. As for the graph of the impedance, we followed the very same procedure of point 1) to obtain the polar plot of Fig.11

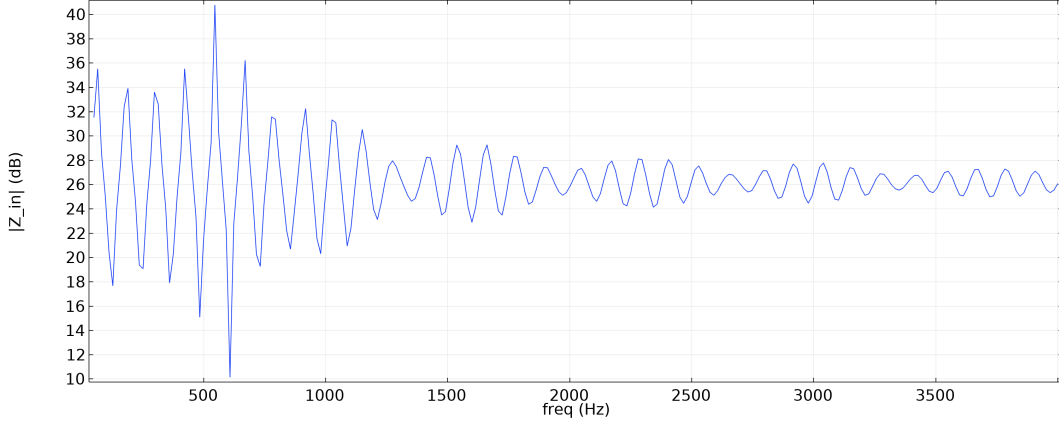


Figure 10: Input impedance of the tube+bell structure

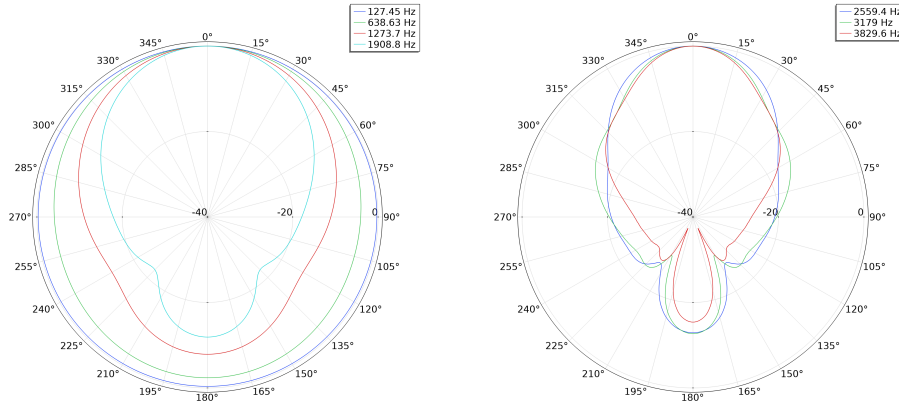


Figure 11: Polar plot of the directivity pattern of the tube+bell structure (first resonance and its multiples of 5 are plotted)

The enhancement in directivity is clear if compared with the tube on its own: in fact, despite at low frequencies the graph may resemble an omnidirectional behaviour, the different scale used corroborate our thesis. Moreover we can observe that the minima of the directivity move from $\pm 30^\circ$ ca. from the rear of the instrument at lower frequencies to $\pm 20^\circ$ for the high end of the spectrum.

3) Mouthpiece

Differently from the bell, in this section we will not add a piece to the instrument, instead we will first study its behaviour when played alone. For what regards the geometry, we used a circular arc of radius rM together with a polygon with short side $rT/8$ and long side rT . The length of the whole piece is Lm ; the parameters used are listed in Fig.12.

Name	Expression	Value	Description
rM	rT+0.3[cm]	0.008 m	Mouthpiece radius
Lm	10[cm]	0.1 m	Length mouthpiece

Figure 12: Simulation parameters for the mouthpiece

The only difference in the volume of air that surrounds the instrument w.r.t. the previous cases is its radius: due to the smaller dimensions of the object to study, we can reduce the circumferences, halving the value of rS . The resulting geometry can be appreciated in Fig.13a, beside which also a particular of the mesh is illustrated: the combination of *Free Triangular* and *Mapped* elements has been kept the same of points 1) and 2). In this case we can notice that very small elements have been used to correctly mesh the narrow part of the mouthpiece, differently from previous models in which larger elements were sufficient to obtain reliable results.

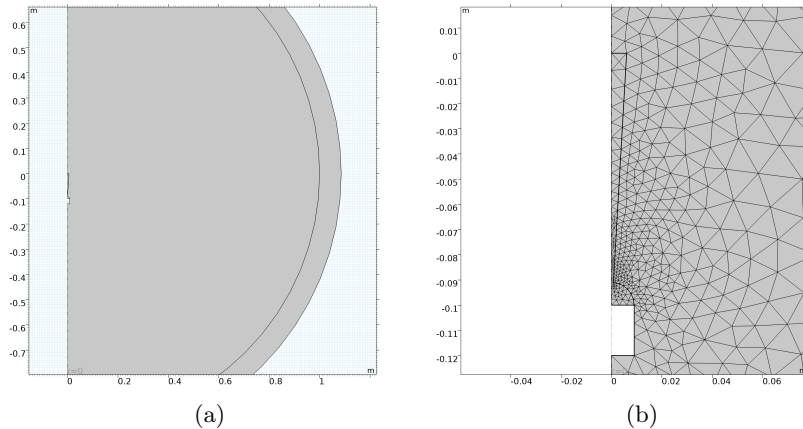


Figure 13: Mouthpiece geometry (a) and mesh (b)

Speaking instead of the physics of the model, we used the usual settings for the input pressure (this time placed on the mouth-hole) and the boundaries of the mouthpiece. The same applies for the *Nonlinear Couplings* and the stored variables. The *Frequency Domain* study in the [50, 4000] Hz range returned the impedance presented in Fig.14.

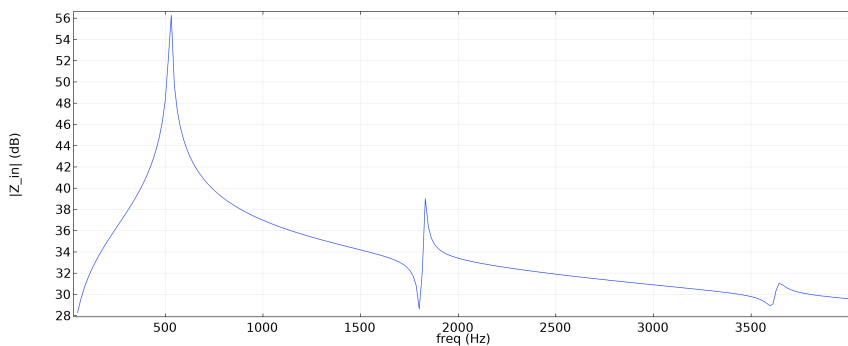


Figure 14: Input impedance of the mouthpiece

The resonances of the system are not harmonically related to each other: the first can

be found at 530.2 Hz, whereas the other two are located at 1831.4 Hz and 3643.7 Hz, progressively attenuated. The trend of the impedance of the mouthpiece resembles that of an Helmholtz resonator, indeed some analogies can be found when comparing the geometries of the two systems. Since the volume V of the cup presents an acoustic compliance $C = V/\rho c^2$ and the constriction behaves as a series inertance $L = \rho l_c/S_c$, we can compute the natural frequency as $\omega_0 = 1/\sqrt{LC}$. This result matches with the well-known expression of the resonance frequency of an Helmholtz resonator if the length l_c and the cross-section S_c of the constriction are correctly defined:

$$f_0 = \frac{c}{2\pi} \sqrt{\frac{S_c}{Vl_c}} \quad (4)$$

Despite these analogies, there are still differences between the two, i.e. the very long neck of the mouthpiece, and the presence of the semi-sphere as an air cavity. These two features of the mouthpiece may lead to a slightly different resonance obtained from the two models.

Finally we can discuss about the directivity of the object, found by plotting the normalized SPL at the boundary of the air volume. From Fig.15 we can immediately see the poor directional properties of the mouthpiece, specially at low frequencies. Indeed, despite the range of the polar plot, only after the second resonance the instrument starts preferring its frontal direction.

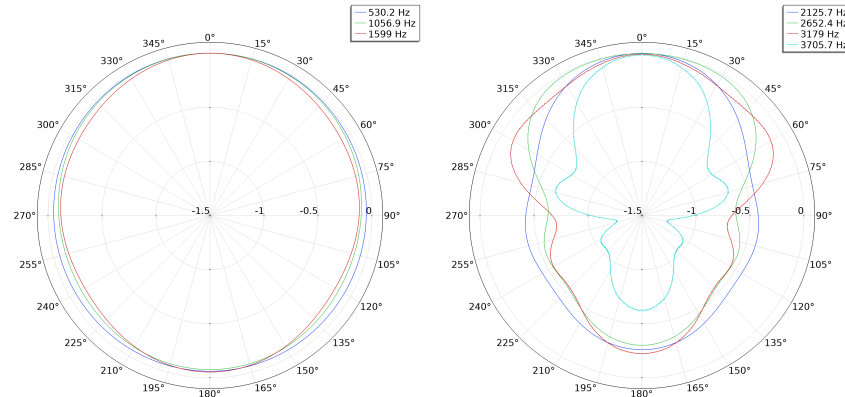


Figure 15: Polar plot of the directivity pattern of the mouthpiece (first resonance and its multiples are plotted)

4) Complete model

For the last point of this report we will combine the three parts of the instrument, hence obtaining an actual trumpet. The geometry of the object is depicted in Fig.16a: notice that for a matter of consistency its exit coincides with the origin. The radius of the air volume has been re-extended to that of the first two exercises due to the dimensions of the subject of the study. The meshing process is consistent with the previous points as well, as can be validated by looking at Fig.16b.

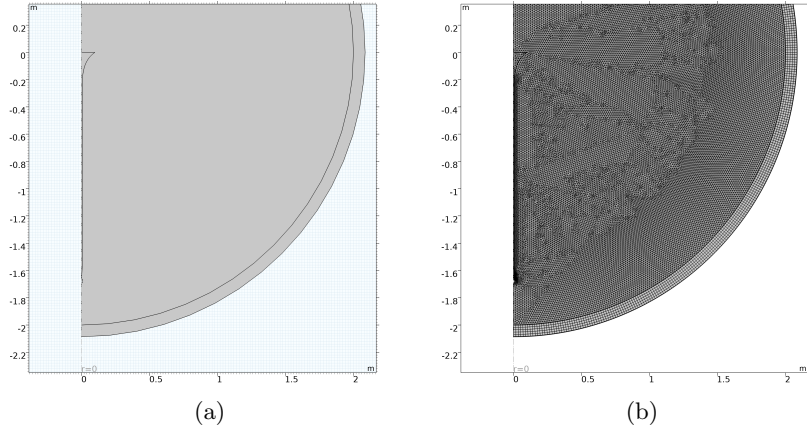


Figure 16: Complete trumpet geometry (a) and mesh (b)

As for the last case, the input pressure is now located on the mouth-hole; while the whole edge of the instrument is characterized by an *Interior Sound Hard Boundaries* physics. After preparing the global variables we can run the study and take a look to the impedance trend reported in Fig.17. The results are clear: the addition of the mouthpiece to the tube+bell structure acts as a filter, enhancing the resonances around 500 Hz and attenuating all the others.

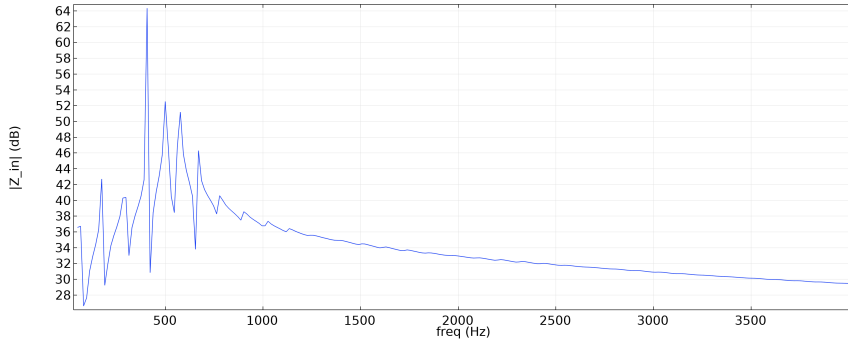


Figure 17: Input impedance of the trumpet

This behaviour is mainly desired because of the way the trumpet is played: the pressure is generated by the lips using the "embouchure" technique, that works at its best when facing a very high impedance system. Consequently the emphasized interval will also correspond to the main playing range of the instrument. At very low frequencies the mitigation introduced by the mouthpiece is not much evident w.r.t. the higher ones, due to the shape of the impedance shown in Fig.10, obtained in section 2) when studying the incomplete trumpet.

The last part of the report is focused on the directivity pattern of the complete model, presented in Fig.18. By looking at the same frequencies investigated in the study of the tube+bell structure, we can immediately notice that the difference is hardly noticeable. We can intuitively state that adding the mouthpiece did not affect the directivity because it applies a change on the input of the instrument, whereas the studied feature mainly concerns its output.

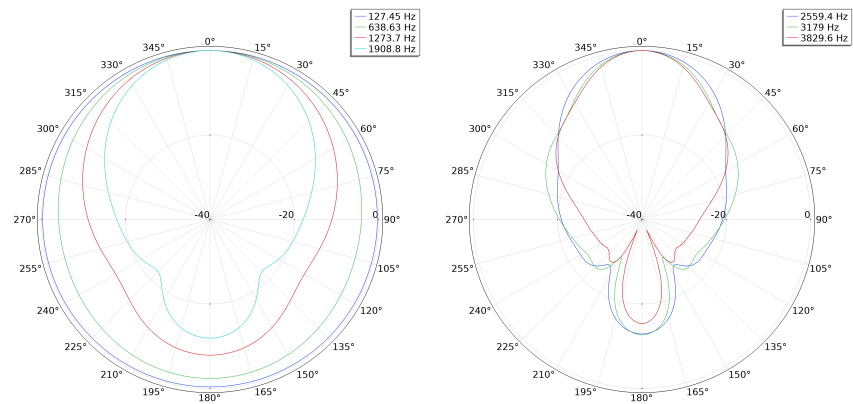


Figure 18: Polar plot of the directivity pattern of the complete trumpet (same frequencies of section 2) are plotted)